



## ULTIMATE SHEAR STRENGTH OF EXISTING STEEL REINFORCED CONCRETE BEAMS WITH LOW-STRENGTH CONCRETE

Kju Kju Nwe (1), Kazushi Sadasue (2), Hideo Araki (3)

<sup>(1)</sup> Graduated student, Hiroshima Institute of Technology, [kknwe.kknwe@gmail.com](mailto:kknwe.kknwe@gmail.com)

<sup>(2)</sup> Associate Professor, Hiroshima Institute of Technology, [sadasue@cc.it-hiroshima.ac.jp](mailto:sadasue@cc.it-hiroshima.ac.jp)

<sup>(3)</sup> Professor, Hiroshima Institute of Technology, [h.araki.k4@it-hiroshima.ac.jp](mailto:h.araki.k4@it-hiroshima.ac.jp)

### **Abstract**

The Japanese archipelago is located in an area where several continental and oceanic plates meet. This is one of the main causes of occurring earthquakes frequently in Japan. In order to prevent disaster of earthquake damages, seismic evaluation and retrofit of existing concrete buildings have been extensive in Japan, after the Hyogoken-Nanbu earthquake (1995). According to some recent seismic evaluation of the existing RC buildings reports, the compression strength of concrete is lower than its applicable lower limit, low-strength concrete. In here, low-strength concrete means the strength of concrete is lower than the applicable limit of 13.5 N/mm<sup>2</sup>, recommended by the Standard for Seismic Evaluation of Existing Concrete Building in Japan.

In this research series, we focus on the Steel Reinforced Concrete structure. This structure is appropriated design to provide a good earthquake resistance structure because it possesses both of the properties of steel and concrete. This Steel Reinforced Concrete structures showed excellent earthquake-resistant capacity under Kanto earthquake (1923), compared with Reinforced Concrete structures. In present day, new building of Steel Reinforced Concrete structure becomes less. But in past, the high-rise buildings of 7stories and more were adopted in the Steel Reinforced Concrete structure by some of the past administration guidance. Although no Steel Reinforced Concrete building had been collapsed by previous earthquake, it was reported that these structure buildings were seriously damaged owing to Hyogoken-Nanbu earthquake (1995). Moreover, these collapsed buildings were reported as the existing buildings, which had been built before the law revision for seismic resistance (1981).

In this experimental research, shear strength of Steel Reinforced Concrete beams were investigated through the seismic loading tests. Considered parameters were rebar type and concrete strength. We focused on the existing high-rise building of Steel Reinforced Concrete beams of low-strength concrete. According to the experimental result, the shear-bond cracks were occurred along the steel flange position when the maximum strength was observed. Furthermore, comparing with the previous research results of Reinforced Concrete beams, Steel Reinforced Concrete beams have excellent deformation capacity, even though low-strength concrete. From the test results, it is found that the ultimate shear strength of low-strength concrete's Steel Reinforced Concrete member cannot be evaluated using the present evaluation method recommended by Japan Building Disaster Prevention Association. Thus, the newly evaluation method for the shear strength of Steel Reinforced Concrete members with low strength concrete can be performed to clarify by the former experiment results, and it is also confirmed that it is reasonable evaluation compared with the result of this experiment, too.

*Keywords: seismic evaluation; low-strength concrete; ultimate shear strength; shear bond failure*



## 1. Introduction

In the “Standard for Seismic Evaluation of Existing Steel Reinforced Concrete Buildings” of Japan Building Disaster Prevention Association [1], the applicable range of concrete compressive strength  $\sigma_B$  is 13.5 N/mm<sup>2</sup> and more is specified. However, it was revealed that the concrete compressive strength of some existing Reinforced Concrete buildings was lower than applicable range, according to the investigation report of existing concrete buildings with low-strength concrete [2]. So, research for seismic efficiency of existing Reinforced Concrete buildings with low-strength concrete was conducted systematically.

By past administration guidance, Steel Reinforced Concrete buildings were adopted for 7 and more stories concrete buildings. So, it can be considered that, the low-strength concrete in existing Steel Reinforced Concrete buildings is also possible. Therefore, we conducted on structural performance of low-strength concrete's SRC columns (full web type of steel frame and open web type of steel frame) and SRC beams (open web type of steel frame) [3]. Throughout the experiment, the ultimate shear strength of present evaluation method, recommended by JBDPA, cannot be evaluated on most of the low-strength concrete's SRC members. Regardless of concrete strength, shear-bond cracks were occurred along the position of strong axis of steel flange for all the SRC columns. Moreover, the hysteresis loop of full web steel frame type SRC columns showed the spindle shape until end of the experiment, but that of open web steel frame type SRC columns became slip characteristics prominently. The fracture type of SRC beams also showed shear-bond cracks, occurred along the position of steel flange. And, the hysteresis loop of open web steel frame type SRC beams also became slip characteristics. In addition, the comparison of brittle behavior between RC columns and SRC columns, with low-strength concrete that were subjected to shear failure, SRC columns were not as brittle as RC columns. It can be confirmed that, SRC columns have excellent deformability and axial force holding ability because steel frame in SRC columns bear the compressive axial force.

In this research, in order to examine the structural characteristics of SRC members with low-strength concrete, carried out the loading test of full web steel frame type SRC beams with low-strength concrete that were subjected to shear failure. Main discussion is concentrated on the structural performance, such as ultimate shear strength and deformation capacity. We also conducted a 3-dimensional finite element method analysis to consider the concrete stress situation of SRC beams.

## 2. Experimental study

### 2.1 Test program detail

Test program and specimen are shown in Table 1 and Fig.1. All specimens were designed as Steel Reinforced Concrete beams, assumed that shear failure precedes flexural failure. It planned a total of 6 specimens with concrete strength (9N/mm<sup>2</sup>, 18 N/mm<sup>2</sup>, 36 N/mm<sup>2</sup>) and type of main rebars (deformed and round) were used as variable.

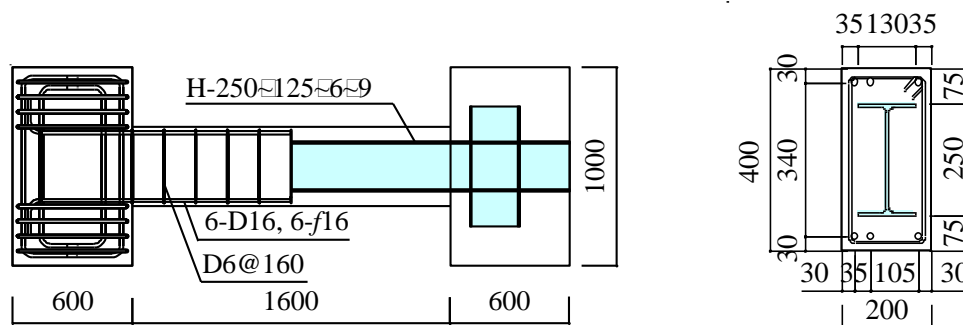


Fig. 1 – Test specimen and cross section (units: mm)



Table 1 – Test program

| Specimen | $F_c$ | Main steel                            | Main rebar                         | Steel shape | Stirrup                      | $M/(Q \cdot d)$ | $b'/b$ |
|----------|-------|---------------------------------------|------------------------------------|-------------|------------------------------|-----------------|--------|
| 36D      | 36    | H-250×125×6×9<br>( $s p_t = 1.41\%$ ) | 6-D16 ( $r p_t = 0.888\%$ )        | Deformed    | D6@100<br>( $p_w = 0.21\%$ ) | 2.00            | 0.38   |
| 36R      |       |                                       | 6- $\phi$ 16 ( $r p_t = 0.897\%$ ) | Round       |                              |                 |        |
| 18D      | 18    |                                       | 6-D16 ( $r p_t = 0.888\%$ )        | Deformed    |                              |                 |        |
| 18R      |       |                                       | 6- $\phi$ 16 ( $r p_t = 0.897\%$ ) | Round       |                              |                 |        |
| 09D      | 9     |                                       | 6-D16 ( $r p_t = 0.888\%$ )        | Deformed    |                              |                 |        |
| 09R      |       |                                       | 6- $\phi$ 16 ( $r p_t = 0.897\%$ ) | Round       |                              |                 |        |

$F_c$ : Design standard strength of concrete ( $\text{N/mm}^2$ ),  $s p_t$ : Tension steel ratio,

$r p_t$ : Tension reinforcement ratio,  $p_w$ : Shear reinforcement ratio,  $M/(Q \cdot d)$ : Shear span ratio,

$b'$ : Effective width of concrete,  $b$ : Column width

In this experiment, cross-section was  $200\text{mm} \times 400\text{mm}$ , type of steel frame was full web type, and used H-250×125×6×9 (SS400) for all specimens, and the band plate was not provided. Main rebar was applied deformed rebars 6-D16 (SR295) for 3 specimens (36D, 18D, 09D), and round rebars 6- $\phi$ 16 (SR295) for the rest (36R, 18R, 09R). The shear reinforcements (stirrup) was D6@160 (SD295A) for all specimens.

The design compressive strength of concrete was set to 3 types of  $9\text{N/mm}^2$ ,  $18\text{N/mm}^2$  and  $36\text{N/mm}^2$ . The mix proportion of concrete is shown in Table 2. And, the stress-strain curve for each strength of concrete is shown in Fig. 2. After reaching the maximum strength, the descending part of  $9\text{N/mm}^2$  showed a very gentle decrease in strength than other ( $18\text{N/mm}^2$ ,  $36\text{N/mm}^2$ ).

Table 2 – Mix proportion of concrete

| $F_c$<br>( $\text{N/mm}^2$ ) | Water<br>( $\text{kg/m}^3$ ) | Cement<br>( $\text{kg/m}^3$ ) | Fine aggregate<br>( $\text{kg/m}^3$ ) | Coarse aggregate<br>( $\text{kg/m}^3$ ) | Admixture<br>( $\text{kg/m}^3$ ) | Water-cement ratio<br>(%) | Fine aggregate ratio<br>(%) |
|------------------------------|------------------------------|-------------------------------|---------------------------------------|---|----------------------------------|---------------------------|-----------------------------|
| 9                            | 205                          | 186                           | 1119                                  | 718                                     | 1.40                             | 110                       | 61.6                        |
| 18                           | 205                          | 234                           | 1079                                  | 718                                     | 1.76                             | 87.6                      | 60.8                        |
| 36                           | 198                          | 384                           | 882                                   | 810                                     | 2.88                             | 51.6                      | 52.9                        |

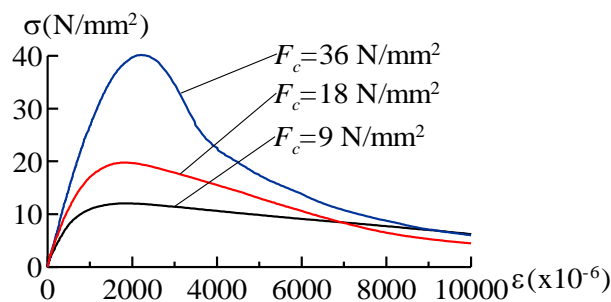


Fig. 2 – Stress-strain curves of concrete



The shear span ratio  $M/(Q.d)$  was 2.0 for all, and the mechanical properties of concrete and steel were shown in Table 3 and Table 4, respectively.

Table 3 – Material properties of steel

| Material             | $\sigma_y$<br>(N/mm <sup>2</sup> ) | $\sigma_u$<br>(N/mm <sup>2</sup> ) | Elongation<br>(%) |
|----------------------|------------------------------------|------------------------------------|-------------------|
| Flange               | 314                                | 438                                | 28.9              |
| Web                  | 345                                | 455                                | 23.6              |
| Main rebar D16       | 342                                | 457                                | 16.6              |
| Main rebar $\phi$ 16 | 321                                | 432                                | 29.2              |
| Stirrup D6           | 331                                | 480                                | 17.1              |

$\sigma_y$ : Yield strength,  $\sigma_u$ : Tensile strength

Table 4 – Material properties of concrete

| Specimen | $F_c$<br>(N/mm <sup>2</sup> ) | $\sigma_B$<br>(N/mm <sup>2</sup> ) | $\sigma_t$<br>(N/mm <sup>2</sup> ) | $E_c$<br>(N/mm <sup>2</sup> ) |
|----------|-------------------------------|------------------------------------|------------------------------------|-------------------------------|
| 36D      | 36                            | 43.2                               | 3.29                               | 30613                         |
| 36R      |                               |                                    |                                    |                               |
| 18D      | 18                            | 20.3                               | 2.11                               | 24652                         |
| 18R      |                               |                                    |                                    |                               |
| 09D      | 9                             | 11.6                               | 1.32                               | 19132                         |
| 09R      |                               |                                    |                                    |                               |

$\sigma_B$ : Compression strength,  $\sigma_t$ : Split tensile strength,  $E_c$ : Young's modulus

## 2.2 Loading principle

All specimens were subjected on the same loading cycle and loading system, shown in Fig. 3. The height of the inflection point of the beams was 800mm, when shear span ratio was 2.0. After fixing the specimen in loading system, loaded repeated-reverse symmetric moment to beam portion. At first, under controlling the displacement of rotation angle  $R$  (relative horizontal displacement between stubs  $\delta$ /interior length  $l$ ), an amplitude of rotation of  $R=\pm 0.125\%$ rad was carried out a cycle. Then, changed in increasing of  $R=\pm 0.25\%$ rad and  $R=\pm 0.50\%$ rad, the next was gradually increased of amplitude by  $R=\pm 0.50\%$ rad to  $R=\pm 2.0\%$ rad, carried out two cycles on every angle. After that, increased of amplitude became  $R=\pm 1.0\%$ rad gradually and carried out two cycles on each angle. The experiment was terminated with up to rotation angle  $I=\pm 5.0\%$ rad of amplitude.

The measurement of stain was measured by stain gauges on H-shaped steel's flange and web, main rebars and shear reinforcements (stirrup), respectively.

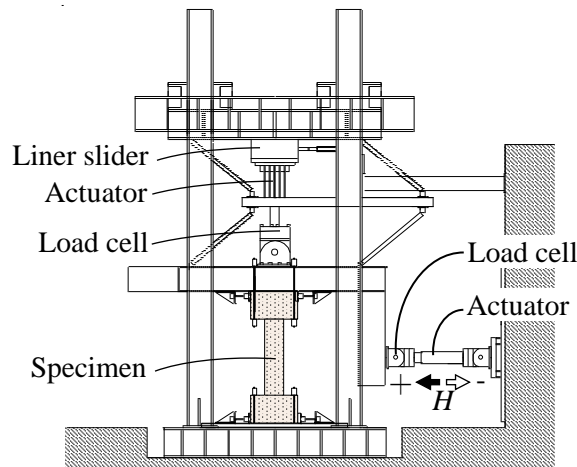


Fig. 3 – Loading system

### 3. Experiment result

The cracks occurrence situation at the end of experiment are shown in Fig. 4. And, the hysteresis loops of specimens, relationship between shear strength  $Q$  and rotation angle  $R$ , are shown in Fig. 5. In Fig.5, the dashed line means the calculated value of ultimate shear strength  $Q_{se}$ , recognized by the seismic performance evaluation standard, and the dotted line means the calculated value of ultimate shear strength  $Q_{se}^*$ , recognized by the proposal method [3]. Moreover, the calculated value of ultimate bending strength exceeds  $Q_{se}$  for all specimens. Hereinafter, the characteristics of failure situation and  $Q$ - $R$  relationship will be described by each specimen, separately.

In 36D ( $F_c=36\text{N/mm}^2$ , deformed rebar), when rotation angle carried out  $R=\pm 0.25\text{rad}$ , both shear-bond cracks occurred along the main rebar and steel flange position, and diagonal cracks also occurred at the both terminal of specimen. From the next rotation, gradual increase of rotation angle  $R$  made shear-bond cracks become expanding to the center of specimen. The maximum strength arrived at the rotation angle  $R=\pm 1.5\text{rad}$ . After the maximum strength, shear-bond cracks increased and expanded widely. Although, it became decreasing the resistance of strength, the hysteresis loop maintained the spindle shape until the end rotation of the experiment.

In 36R ( $F_c=36\text{N/mm}^2$ , round rebar), diagonal cracks occurred at both terminal sides of the specimen when amplitude of rotation angle  $R=\pm 0.25\text{rad}$ . When rotation angle carried out  $R=\pm 1.0\text{rad}$ , shear-bond cracks occurred along the main rebar and steel flange position. After that, cracks increased and expanded widely by increasing the amplitude of rotation angle  $R$ . However, it did not reach ultimate shear strength for this 36R specimen, until the end of experiment, with maintaining the hysteresis loop as spindle shape.

In 18D ( $F_c=18\text{N/mm}^2$ , deformed rebar), diagonal cracks occurred at both terminal sides of the specimen when amplitude of rotation angle  $R=\pm 0.125\text{rad}$ . When rotation angle carried out  $R=\pm 0.25\text{rad}$ , shear-bond cracks occurred along the main rebar and steel flange position. At the amplitude of rotation angle  $R=\pm 0.5\text{rad}$ , shear-bond cracks become expanding to the center of specimen. The maximum strength arrived at the rotation angle  $R=\pm 1.0\text{rad}$ . After that, both diagonal cracks and shear-bond cracks increased and expanded widely almost the entire surface. Although, it showed resistance of strength decay once after maximum strength, the strength tended to increase as rotation angle increased. Moreover, the hysteresis loop maintained the spindle shape until the end rotation of the experiment.

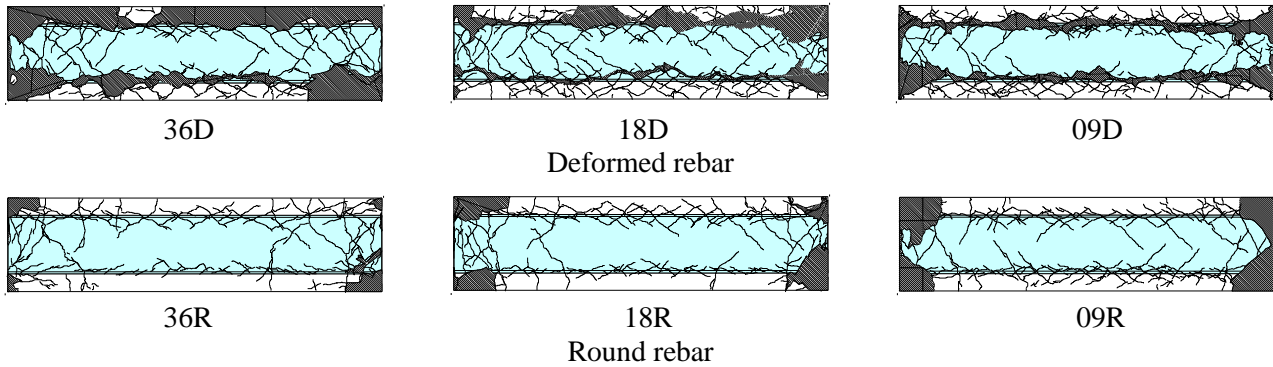


Fig. 4 – Final failure state

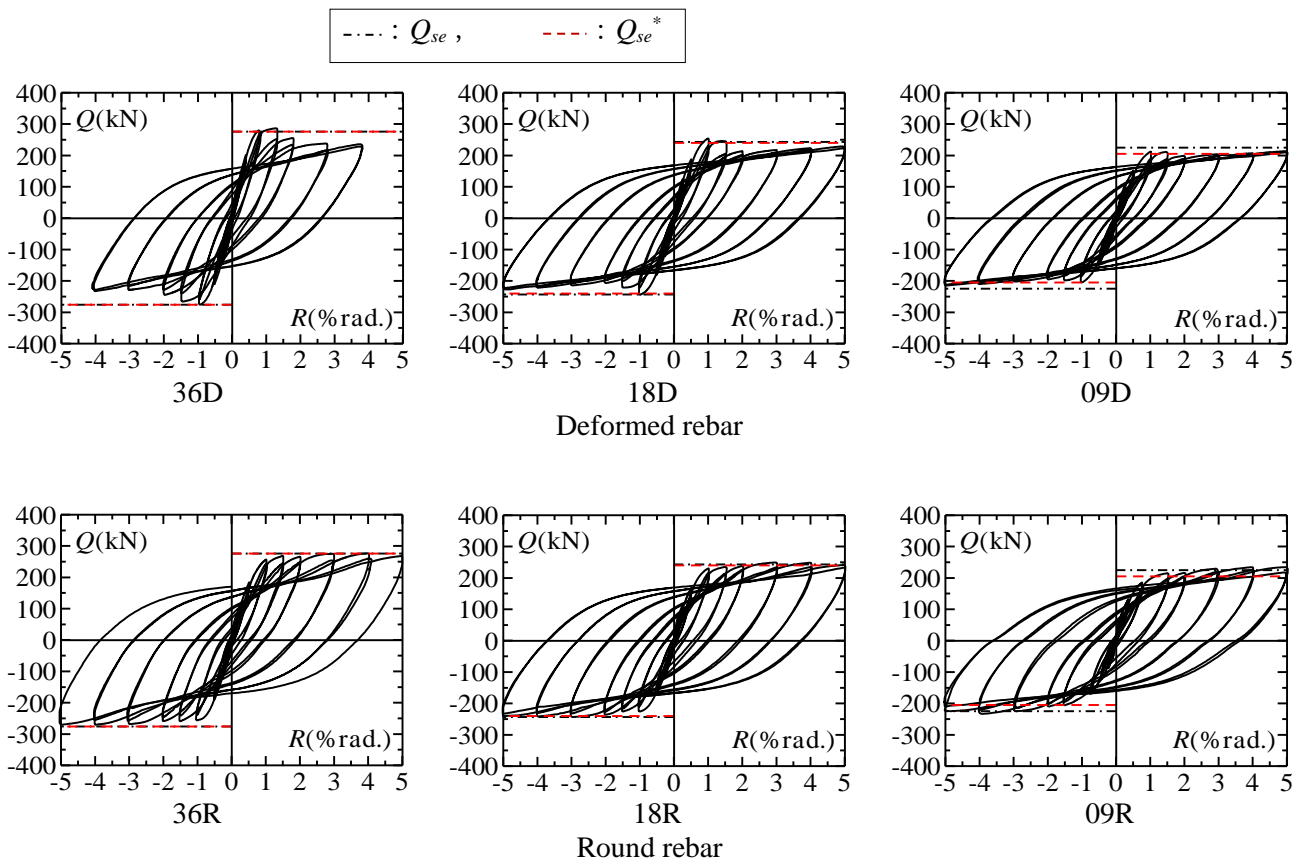


Fig. 5 – Hysteresis loop

In 18R ( $F_c=18\text{N/mm}^2$ , round rebar), when rotation angle carried out  $R=\pm 0.25\%$ rad, both shear-bond cracks occurred along the main rebar and steel flange position, and diagonal cracks also occurred at the both terminal of specimen. From  $R=\pm 0.50\%$ rad rotation angle, gradual increase of rotation angle  $R$  made shear-bond cracks become expending to the center of specimen. The maximum shear strength was reached at an amplitude of  $R=\pm 3.0\%$ rad. However, the strength maintained constantly as maximum strength until the end of the experiment, and the hysteresis loop also maintained the spindle shape as above specimens.

In 09D ( $F_c=9\text{N/mm}^2$ , deformed rebar), when rotation angle carried out  $R=\pm 0.25\%$ rad, both shear-bond cracks occurred along the main rebar and steel flange position, and diagonal cracks also occurred at the both



terminal of specimen. The next amplitude of rotation angle  $R=\pm 0.50\%$ rad, shear-bond cracks become expending to the center of specimen. The maximum strength arrived at the rotation angle  $R=\pm 1.5\%$ rad. After that, shear-bond cracks increased and expanded widely. Although, it showed resistance of strength decay once after maximum strength, the strength tended to increase as rotation angle increased. Moreover, the hysteresis loop maintained the spindle shape until the end rotation of the experiment.

In 09R ( $F_c=9\text{N/mm}^2$ , round rebar), diagonal cracks occurred at both terminal sides of the specimen when amplitude of rotation angle  $R=\pm 0.25\%$ rad. When rotation angle carried out  $R=\pm 0.50\%$ rad, shear-bond cracks occurred along the main rebar and steel flange position. After that, cracks increased and expanded widely by increasing the amplitude of rotation angle  $R$ . However, it did not reach ultimate shear strength for this 09R specimen, until the end of experiment, with maintaining the hysteresis loop as spindle shape.

Comparison between the experimental results of SRC beams using deformed rebar and SRC beams using round rebar, the shapes of hysteresis loop were seemed almost the same. But, the aspects of failure behavior were seemed different. Moreover, deformed rebars yielded at rotation angle  $R=\pm 1.0\%$ rad, but round rebars did not yield until the end.

Comparison between the maximum value of experimental result  $Q_{exp}$  and calculated value of evaluation method  $Q_{se}$ , it can recognize that  $Q_{exp}>Q_{se}$  while  $\sigma_B\geq 13.5\text{N/mm}^2$ . But, the specimens with  $\sigma_B<13.5\text{N/mm}^2$ , 09D was  $Q_{exp}<Q_{se}$  and 09D was also confirmed  $Q_{exp}$  is larger than  $Q_{se}$  while reaching to large deformation rotation angle  $R=\pm 3.0\%$ rad. On the other hand, calculated value of proposal method  $Q_{se}^*$  is confirmed as stability condition of  $Q_{exp}\leq Q_{se}^*$  for all specimens' experimental result  $Q_{exp}$ .

## 4. Ultimate shear strength

### 4.1 Seismic evaluation criteria method of ultimate shear strength $Q_{se}$

The ultimate shear strength criteria method  $Q_{se}$  is applied on the JBDPA, standard for structural calculation of existing Steel Reinforced Concrete buildings. It is based on the applicable compressive strength of concrete is  $13.5\text{N/mm}^2$  and more. Eq. (1) shows the criteria method for full web type beam, and it is calculated by adding the strength of steel part to the strength of reinforced concrete part, based on Arakawa (min) equation.

$$Q_{se} = \left\{ \frac{0.053 r p_t^{0.23} k_{cs} (18 + F_c)}{M/(Q \cdot d) + 0.12} + 0.85 \sqrt{r p_w \cdot r \sigma_{wy}} \cdot b \cdot j \right\} + s Q_u \quad (1)$$

$$k_{cs} = \frac{b'}{b} + 0.5 \quad (\text{Except; } k_{cs} \leq 1.0) \quad (2)$$

where,  $r p_t$  is tensile main rebar ratio,  $r \sigma_{wy}$  is yield strength of reinforcement,  $j$  is distance between tensile and compressive resistant of reinforced concrete,  $b$  is width of column,  $b'$  is effective width of concrete. And,  $s Q_u$  in Eq. (1) is the minimum value of ultimate flexural strength  $s Q_{mu}$  and ultimate shear strength  $s Q_{su}$ , when the axial force of steel portion set to "0". Moreover,  $k_{cs}$  is reduction coefficient against the strength of concrete for direct shear failure on steel flange and shown in Eq. (2).

A comparison between the maximize strength of experiment  $Q_{exp}$  and calculated value of ultimate shear strength method Eq. (1)  $Q_{se}$  is shown in Table 5. And, while using experiment value  $Q_{exp}$  in Y-axis and calculated value  $Q_{se}$  in X-axis, the results of  $Q_{exp}$  and  $Q_{se}$  for all SRC beams, carried out in this research and previous research in plot graph is shown in Fig. 6(a).

The seismic evaluation criteria method is applied by Arakawa (min) equation, based on the experimental results which were using concrete strength is more than applicable range  $13.5 \text{ N/mm}^2$ . In this



research, specimen with low-strength concrete beams 09D showed experimental value was lower than calculated value. As same as the report of previous research of reinforced concrete and steel reinforced concrete members with low-strength concrete in Ref. [2] and [3], 09D specimen (using deformed rebar and 9N/mm<sup>2</sup> concrete) was confirmed as instability condition by this criterion.

Table 5 – Experiment and calculated value

| Specimen | $Q_{exp}$<br>(kN) | $Q_{se}$<br>(kN) | $Q_{se}^*$<br>(kN) | $Q_{exp}/Q_{se}$ | $Q_{exp}/Q_{se}^*$ |
|----------|-------------------|------------------|--------------------|------------------|--------------------|
| 36D      | 287               | 276              | 276                | 1.04             | 1.04               |
| 36R      | 277               |                  |                    | 1.00             | 1.00               |
| 18D      | 254               | 243              | 240                | 1.05             | 1.06               |
| 18R      | 249               |                  |                    | 1.02             | 1.04               |
| 09D      | 214               | 227              | 205                | 0.94             | 1.04               |
| 09R      | 216               |                  |                    | 0.95             | 1.05               |

full web type)  $\triangle$ :  $\geq F_c 13.5\text{N/mm}^2$ ,  $\blacktriangle$ :  $< F_c 13.5\text{N/mm}^2$ ; open web type)  $\circ$ :  $\geq F_c 13.5\text{N/mm}^2$ ,  $\bullet$ :  $< F_c 13.5\text{N/mm}^2$

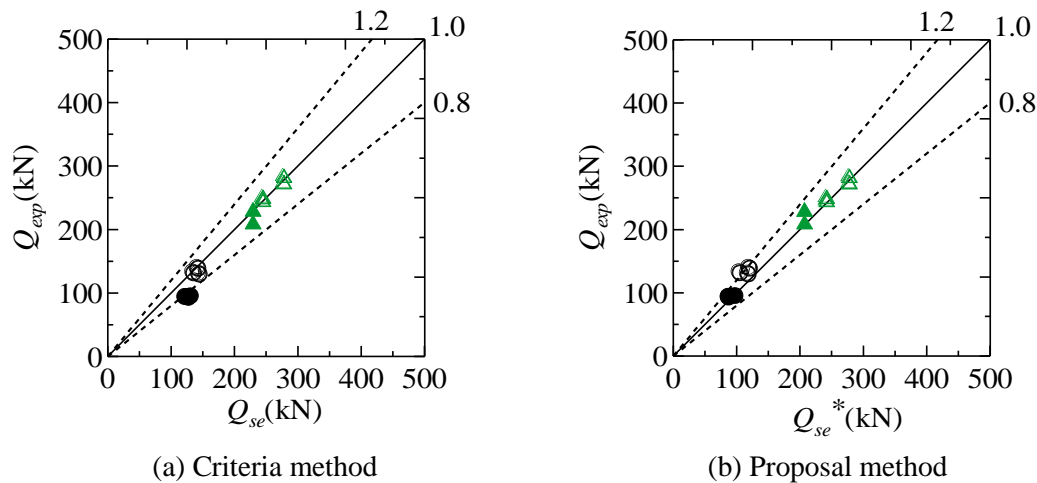


Fig. 6 – Experiment result with criteria method result verse experiment result with proposal method result

#### 4.1 Proposal method of ultimate shear strength $Q_{se}^*$

In the ultimate shear strength equation of Steel Reinforced Concrete seismic evaluation criteria  $Q_{se}$ , most of specimens of experimental value confirmed as instability condition, especially in low-strength concrete, using concrete strength is lower than applicable range of concrete compressive strength 13.5N/mm<sup>2</sup>. By this reason, we applied the ultimate shear strength equation of Steel Reinforced Concrete members  $Q_{se}^*$ , that can also be able to express applicable to low-strength concrete, has been provided in previous research [3]. Regardless of using shape of steel and type of rebar, proposal equation can calculate as Eq. (1), Eq. (3) and Eq. (4). The value of  $k_{cs}$  is expressed as a function of  $b'/b$  with 0.5, and multiplies  $b'/b$  with reduction coefficient of concrete strength  $\beta_L$ . Exception, the limit of  $k_{cs}$  is from 0.27 to 1.0.

$$k_{cs} = \beta_L \cdot \frac{b'}{b} + 0.5 \quad (\text{Except; } 0.27 \leq k_{cs} \leq 1.0) \quad (3)$$



$$\beta_L = \frac{1.27}{9} \cdot \sigma_B - 1.27 \quad (4)$$

As same as  $Q_{se}$ , comparison between the maximize strength of experiment  $Q_{exp}$  and calculated value of  $Q_{se}^*$  is shown in Table 5. Meanwhile, using experiment value  $Q_{exp}$  in Y-axis and calculated value  $Q_{se}^*$  in X-axis, the results of  $Q_{exp}$  and  $Q_{se}^*$  for all SRC beams, carried out in this research and previous research in plot graph is shown in Fig. 6(b).

In this applicable to low-strength concrete proposal equation  $Q_{se}^*$ , variance of comparison is smaller than criteria method  $Q_{se}$ , and all Steel Reinforced Concrete specimens were shown in stability condition, as over than experimental results. So, it can be confirmed that it is reasonable evaluation compared with the result of experiment.

## 5. Simulation of Finite Element Method analysis (FEM analysis)

In this research, we also perform a simulation of 3 dimensional Finite Element Method analysis (FEM analysis) [4]. And, the result of FEM analysis is verified by comparing with the experimental work.

### 5.1 Simulation model

The simulation model is shown in Fig. 7, established the 1/2 of experimental Steel Reinforced Concrete beam, which can not only reduce the calculation time but also avoid terminating the calculation process du to too many warnings. The loading system is based on experimental work, such as loading repeated-reverse symmetric moment to beam portion up to rotation angle  $R=\pm 5.0\%$ rad of amplitude, but is carried out one cycle for each rotation. Fig. 7 shows concrete and steel elements mesh model in stub portion and concrete elements mesh model in specimen portion, steel frame element mesh model and rebar element model, respectively.

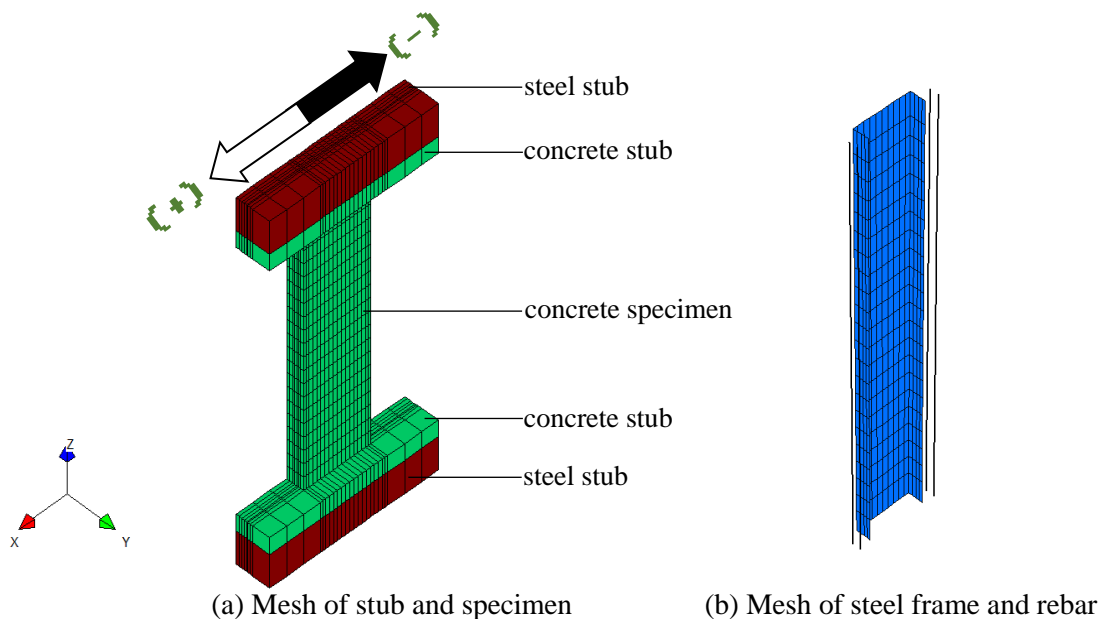


Fig. 7– Element model of separate materials

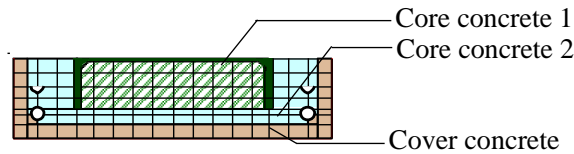
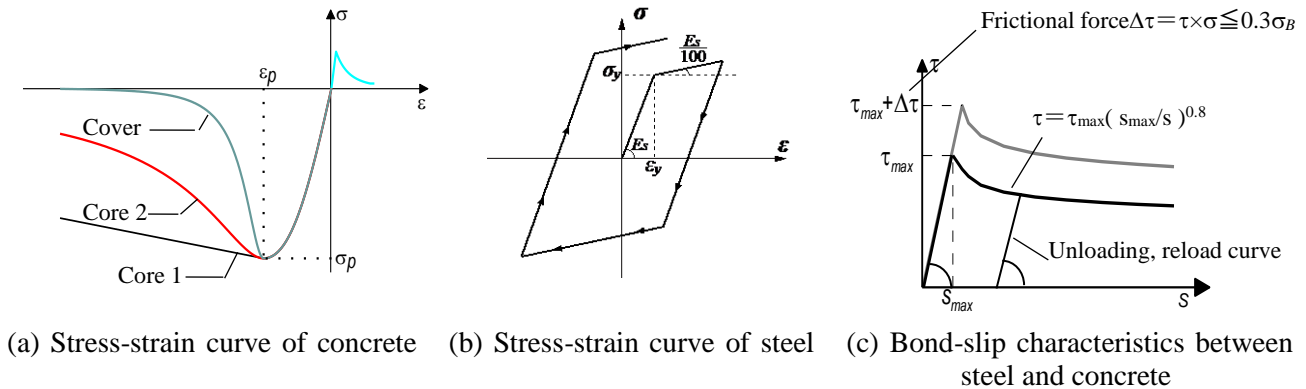


Fig. 8- Element types of concrete



(a) Stress-strain curve of concrete (b) Stress-strain curve of steel (c) Bond-slip characteristics between steel and concrete

Fig. 9- Constitutive law

## 5.2 Configuration model of specimen portion

Concrete mesh was modeled in hexahedral element, and type of concrete elements, separated by positioning of steel frame, is shown in Fig. 8. As shown in Fig. 9(a), the constitutive law of concrete in compression side for the increased area, up to the yield point was using Correction Ahmad model [5], while for descending area, after the yield point was using Nakamura model [6] for core concrete 1 slope (means concrete elements inner the steel frame), Correction Ahmad model for core concrete 2 slope (means concrete elements between steel frame and shear reinforcement) and cover concrete model for cover concrete slope (means concrete elements outside of shear reinforcement). On the other side, concrete in tensile side, up to tensile stress area was using linear model, while descending area was Izumo model, which was tensile hardening model.

Rebar was modeled in truss element. Meanwhile, shear reinforcement (stirrup) was modeled as embedded reinforcement model. The stress- strain curve for both deformed rebar and round rebar expressed in bilinear model, and is shown in Fig. 9(b). The yield condition of rebar was expressed in Von Mises's condition, then, the hysteresis characteristics was used in isotropic hardening law.

Steel was modeled in quadrilateral element, furthermore, plate stress model in steel web and combination shell stress model in steel flange, because flange is thicker. As shown in Fig. 9(b), stress-strain curve for steel was expressed in bilinear model such as rebar. Moreover, yield condition of steel was expressed in Von Mises's condition, then, the hysteresis characteristics was used in isotropic hardening law.

As shown in Fig. 9(c), the bond-slip characteristics of adhesion between steel and concrete was based on Kin's research [8] in linear model until maximum bond strength, and Amano's research [9] in curving multi linear model after maximum strength. And then, the bond-slip characteristics of adhesion between rebar and concrete was Elmorsi model [10] for deformed rebar, while using the same system for steel in round rebar.

## 5.3 Comparison result of FEM analysis with experimental work

Fig. 10 shows the hysteresis loops of each specimen FEM analysis in dashed line and experiment in continuous line. As same as Fig. 5, X-axis shows rotation angle  $R$  and Y-axis shows shear strength  $Q$ .



Regarding the  $Q$ - $R$  relationship, the skeletal line in both of Steel Reinforced Concrete beams with low-strength concrete were seemed as well correspondence until end of the loading. Furthermore, the analytical values of FEM analysis can express the experimental values almost accurately.

With respect to the effect of rebar, the comparison of strength up to rotation angle  $R=2.0\%$  rad showed the FEM analysis strength was lower than experiment, but the strength tended to increase as rotation angle increased in using deformed rebar specimens. In the case of round rebar specimens, it can be confirmed that the analytical values could accurately evaluate the experimental values, except 36R.

For all specimens, showed the different behavior from experiment while the hysteresis loops swelled outward as rotation angle increased. It can be considered, it seems to required further study on the bond-slip characteristics between steel and concrete members.

And, compressive stress distribution of FEM analysis of concrete portion can be confirmed that compression status were formed diagonally at the specimen terminal part. Furthermore, due to surround by steel frame, concrete core1 had higher stress resistance than the rest 2 types.

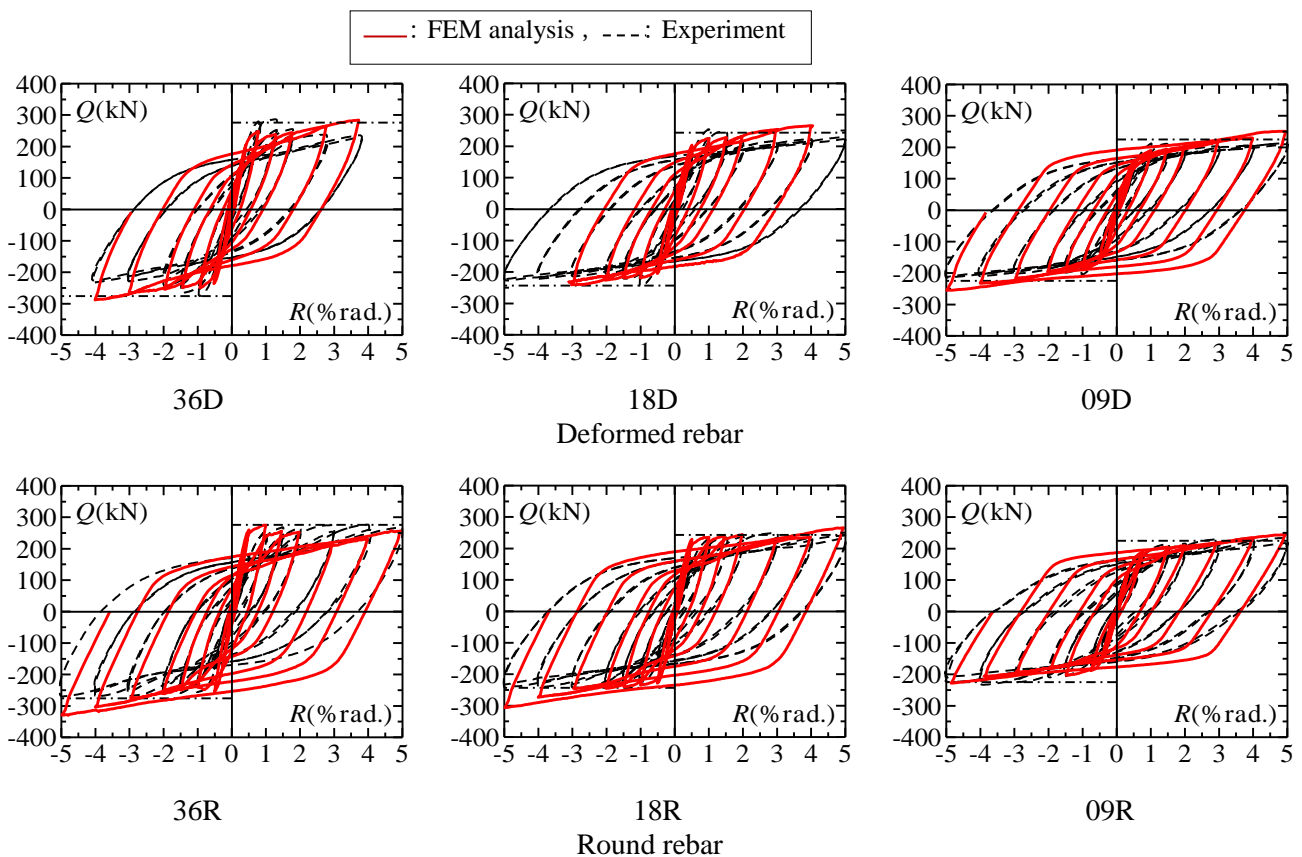


Fig. 10– Comparison of the results of experimental with FEM analysis by hysteresis loops



## 6. Conclusions

Through the above experiment and FEM analysis, the following conclusions can be drawn.

- (1) Regardless of the concrete strength and types of main rebar, final failure conditions expressed that the shear-bond cracks were occurred along the main rebar and steel flange position.
- (2) The ultimate shear strength maintained constantly as maximum strength until the end of the experiment in Steel Reinforced Concrete beams with round rebar, and slightly decreased after maximum strength in beams with deformed rebar.
- (3) Comparison between the maximum value of experimental result  $Q_{exp}$  and calculated value of evaluation method  $Q_{se}$ , it resulted  $Q_{exp} < Q_{se}$  when  $\sigma_B < 13.5 \text{ N/mm}^2$ . But, the calculated value of proposal method  $Q_{se}^*$  is confirmed as stability condition of  $Q_{exp} \leq Q_{se}^*$  for all specimens' experimental result  $Q_{exp}$ .
- (4) In FEM analysis of Steel Reinforced Concrete Beams, the analytical values of FEM analysis can express the experimental values almost accurately especially in specimens with low-strength concrete.
- (5) In FEM analysis, the hysteresis loops swelled outward of experimental results and it seems to required further study on the bond-slip characteristics between steel and concrete members.

## 7. Acknowledgements

We would like to show our gratitude to JSPS grant-in-aid for scientific research (issue number: JP16H04458) and 2017 grant research of Japan Concrete Institute, for being funded and supported this research.

## 8. References

- [1] Standard for Seismic Evaluation of Existing Steel Reinforced Concrete Buildings (2009): The Japanese Building Disaster Preventing, (in Japanese)
- [2] Symposium of Seismic Evaluation and Retrofitting of Existing Buildings with Low-Strength Concrete (2013): Japan Concrete Institute, Chugoku Branch
- [3] Kju Kju New, Kazushi Sadasue, Hideo Araki (2019): Ultimate shear strength of existing steel reinforced concrete members with Low-strength concrete, *Journal of Structural and Construction Engineering by Architectural Institute of Japan*, 84 (761), 983-992
- [4] Ito Chu Techno-solution Co.,Ltd.: FINAL/V11 HELP
- [5] Naganuma K (1995): Stress-strain relationship of concrete under triaxle compression, *Journal of Structural and Construction Engineering by Architectural Institute of Japan*, 474, 163-170
- [6] Nakamura H, Higai T (1999): Compressive Fracture Energy and Fracture Zone Length of Concrete, Seminar on Post-peak Behavior of RC Structures Subjected to Seismic Load, JCI-C52E, 2, 259-272
- [7] Matsui T, Kuramoto H (2008): Stress transferring mechanisms of composite CES beam-column joint under lateral load reversals, *Journal of Structural and Construction Engineering by Architectural Institute of Japan*, 73 (630), 1401-1408
- [8] Kou K, Yonezawa K, Noguchi H (1994): Experimental study on bond characteristics of steel and concrete composite structure, *Summaries of Technical Reports of Annual Meeting by Japan Concrete Institute*, C2, 1631-1632
- [9] Amano O, Nakamura H, Hikai I (1998): Analysis of Shear behavior on steel pipe and concrete composite pier, *Summaries of Technical Papers of Annual Meeting by Architectural Institute of Japan*, 20 (3), 823-828
- [10] Elmsori, M. et al. (1971): Flexural Members with Confined Concrete, *Journal of the Structural Division, ASCE*, 97, 1969-1990